Available online at www.sciencedirect.com
SCIENCE DIRECT
Journal of Power Sources 156 (2006) 78–84
JOURNAL OF POWER SOURCES
www.elsevier.com/locate/jpowsour

Thermal management of a PEMFC stack by 3D nodal modeling

L. Dumercy [a,*], R. Glises [a], H. Louahlia-Gualous [b], J.M. Kauffmann [a]

[a] *Laboratoire de Recherche en Electronique, Electrotechnique et Systèmes (L2ES), UFC-UTBM EA 3898, Rue T. MIEG, 90010 Belfort cedex, France*
[b] *FEMTO-ST, CNRS UMR6174, CREST, 2 av. Jean Moulin, 90000 Belfort, France*

Available online 14 February 2006

Abstract

This paper describes a 3D thermal modeling by a nodes network model for two PEMFC of 150 and 500 W (respectively, 3 and 20 cells). Modeling are realized for each case for one cell before to be integrated on all the stack. Absolute temperatures of H_2, air and water channels are used as Dirichlet conditions. Temperatures of external surfaces are obtained thanks to an infrared thermographic camera. Final external heat fluxes are deduced from the integrated model.

Keywords: Fuel cells; Thermal model; Nodes network

1. Introduction

Operating conditions of a fuel cell widely depend on the thermal management. It is used to control the cooling system, to maintain a good hygrometry level in the fuel cell and to optimize the global efficiency of the system. Some studies concerning the solid structures have been made by considering isothermal cells. Then, the computations of the temperatures are obtained in the fluids of the ducts [1]. Other studies are made where the distribution of temperatures is computed on the working plates [2], but the gradients of temperature through the layers (MEA) are not taken into account, then the heat transfer can only be estimated along the channels. These studies are realized with two kinds of boundary conditions: free convection or with a water circulation on the external faces (forced convection). 3D thermal computations are done considering the imposed temperatures of the working plates as Dirichlet boundary conditions [3,4]. The main object of this work is to study the influence of temperature on physical parameters as for example, the hygrometry rate of the membrane. The cooling system is not taken into account. All these works focused on different parts of one cell. This latter is not considered as an entire unit. Different ways where the cell evacuates the produced heat power are studied to establish a thermal management. So the thermal flux paths must be known and particularly the part of the heat which must be removed by the cooling system or transferred by conduction–convection across the faces of the stack. It is necessary to know the ability of the heat fluxes to cross through the cells and to quantify the part concentrated in the bipolar plates and dissipated on the external surfaces. This study uses a 3D thermal nodes network to compute the temperatures and the flux distribution in the cell. Various boundary conditions are applied, cyclic or imposed flux to study the thermal operating mode between two adjoining cells or the heat transfer along the length of the stack. The distribution of temperatures is obtained for different current densities for two stacks respectively of 150 W (3 cells) and 500 W (20 cells). The surface temperature is supposed as constant and defined by the cooling system whose temperature is controlled at the output and the heat transfer through the faces is also constant. The heat flux extracted by the cooling system is therefore greatly depending on the current density. Comparisons with experiments are presented.

2. Thermal modeling by 3D nodal network

The modeling of the solid structure of one cell (14 cm × 14 cm × 0.3 cm) is carried out with a nodal network consisted of 172 nodes (temperatures of the wall are measured and used as boundary condition) or 236 nodes (temperatures of

* Corresponding author at: Centre de Recherche sur les Ecoulements, Surfaces et Transferts (CREST), FEMTO ST UMR CNRS 6174, Parc Technologique, 2 Rue Jean Moulin, 90000 Belfort, France.
E-mail address: laurent.dumercy@utbm.fr (L. Dumercy).

0378-7753/$ – see front matter © 2005 Elsevier B.V. All rights reserved.
doi:10.1016/j.jpowsour.2005.08.038

Nomenclature

a	$m^2\,s^{-1}$
C	$J\,K^{-1}$
F	$C\,mol^{-1}$
g	$m\,s^{-2}$
G	$W\,K^{-1}$
Gr	Dimensionless
h	$W\,m^{-1}\,K^{-1}$
ΔH	$J\,mol^{-1}$
I	A
Nu	Dimensionless
$P_{chemical}$	W
$P_{electrical}$	W
Pr	Dimensionless
$P_{thermal}$	W
Q	W
Ra	Dimensionless
Re	Dimensionless
T	K
U	V
u_m	$m\,s^{-1}$
x	M

Greek symbols

β	K^{-1}
λ_{fl}	$W\,K^{-1}\,m^{-1}$
ν	$m^2\,s^{-1}$
ζ	Dimensionless

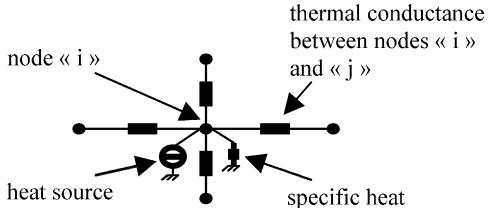

Fig. 1. Elements of the nodal network.

the wall are computed) of volume and surface. The nodes represent heat and mass transfer between fluid and solid interfaces [5]. Fig. 1 shows a typical node with its thermal conductances, each of them can represent radiation, convection, conduction and/or mass transfer with surrounding nodes.

In the modeling, radiation is not taken into account considering the low temperature levels. Heat power sources are electrochemical reactions of the production of H_2O in the cathode channel. Eq. (1) is the thermal balance for the node "i" given for 1–172 (236 when including nodes of the fluids). In this equation, $G_{i,j}$ represents a "conductance" in $W\,K^{-1}$ which is the inverse of the thermal resistance:

$$C_i \frac{dT_i}{dt} = \sum_j G_{i,j}(T_j - T_i) + Q_i \quad (1)$$

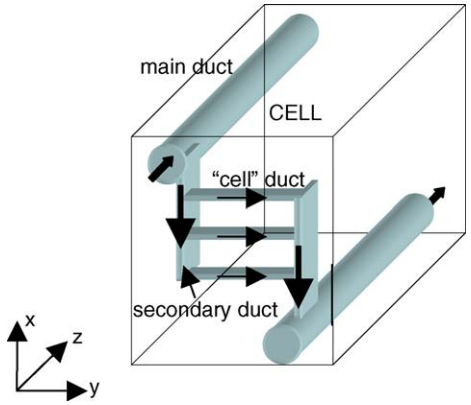

Fig. 2. Description of the cooling system.

Table 1
Hydraulic diameters for the cooling system

Main duct (mm)	7.1
Secondary duct (mm)	3.5
Cell duct (mm)	0.8

With the different expressions of conductances given by Eqs. (2a)–(2c):

$$G_{i,j} = \lambda_k \frac{S_{i,j}}{L_{i,j}} \quad (2a)$$

$$G_{i,j} = h_{i,j} S_{i,j} \quad (2b)$$

$$G_{i,j} = \dot{m} c_p \quad (2c)$$

λ_k is the thermal conductivity of the material "k". $L_{i,j}$ and $S_{i,j}$ are respectively the distance and the heat exchange surface between nodes i and j. $h_{i,j}$ the coefficient of convection at the interface $S_{i,j}$, m the mass flow ($kg\,s^{-1}$) and c_p the specific heat ($J\,kg^{-1}\,K^{-1}$).

The final system to solve also consists of 172 or 236 analytical equations [6], respectively for the 3 and 20 cells. The system is then transformed into an equation composed of matrix and vectors and solved with a Gear method thanks to the mathematical software MATLAB.

The nodal modeling is carried out for only one cell of the PEMFC. Internal Dirichlet boundary conditions are obtained thanks to the input temperatures of the water cooling system (K thermocouple at the entrance of the stack).

Fig. 2 represents the simplified cooling system which uses demineralized water. As shown in this figure, modeling of the channels is significantly simplified with only three ducts instead of the real geometry. This choice is justified by the compromise between the satisfying accuracy on the temperature distribution and the shorter duration of computation determined by the number of nodes. However, the really mass fluxes are taken into account and adapted transfer surfaces are considered with equivalent hydraulic diameters given in Table 1.

3. Model implementation

Fig. 3 describes the developed model. The modeled water channels are represented as channels 1–3. These nodal "con-

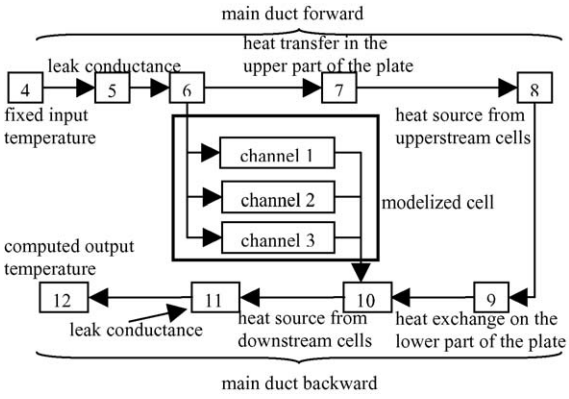

Fig. 3. Different parts of the modeling of the cooling system.

ductances" characterize heat transfer by convection between the fluid and the surrounding solid surfaces so that the mass transfer exists along the duct. Conductance 4 is the Dirichlet condition imposed at the input of the cooling channel at the entrance of the stack. The input temperature of the water is represented with the conductance 12.

Its value is calculated and compared to the experimental value obtained thanks to a thermocouple of the test bench. Convergence between the simulated and the experimental temperature is obtained by modifications of the leak conductances 11 and/or 5. It represents the external heat losses of the modeled cell. Conductances 7 and 10 represent the heat fluxes of the studied cell with the surrounding air. Finally, conductances 8 and 10 represent the thermal influence of the neighboring cells. They permit to consider the thermal sources and/or the conduction losses in the third dimension (axis O, z).

4. Boundary conditions

Three configurations of modeling have been considered for the studied cell. Differences come from different applications of boundary conditions. First, applied boundary conditions have to represent the heat fluxes (B.C. First kind) between different associated cells. The other applied boundary conditions on the external surfaces are first kind boundary conditions of Dirichlet (absolute temperature) [7]. The knowledge (or not) of these lasts is at the origin of a two different configurations.

- *Configuration* 1. Thermal flux lost on one interface is gained on the opposite one. The absolute temperatures on the external surface are known.
- *Configuration* 2. Thermal flux lost on one interface is gained on the opposite one but the temperatures on the external surfaces are unknown and finally obtained thanks to an iterative process.
- *Configuration* 3. Thermal flux which is transferred on the first interface can be different from the one transferred on the opposite interface. Both values are algebraic expressions. The external temperatures are obtained as for configuration 2.

Absolute temperatures (Dirichlet conditions) on the external surfaces are obtained thanks to an infrared short waves camera (case 1 of chapter results). The emissivities of the external surfaces are obtained by comparison and convergence of the temperature obtained with a thermocouple and the other one obtained by radiation. The convergence is obtained for an emissivity of all surfaces at 0.94. These temperatures can be used as boundary conditions. It is possible, as done in this study, to used them only to valid the model by comparison of the final surface computed temperatures with the temperatures obtained by radiation measurement.

5. Equations

To define the conductances and the thermal resistances, it is necessary to know all internal power sources. In that way, chemical energy released by consummation of hydrogen is given by Eq. (3):

$$P_{\text{chemical}} = \Delta H_{\text{H}_2\text{Og}} \frac{I}{2F} \tag{3}$$

Eq. (4) gives the electric energy supplied to the load:

$$P_{\text{electrical}} = UI \tag{4}$$

Finally, internal thermal power source is equal to the difference between (3) and (4) is shown by Eq. (5):

$$P_{\text{thermal}} = P_{\text{chemical}} - P_{\text{electrical}} \tag{5}$$

Thermal conductivities used for the modeling are given in Table 2.

Different correlations are used to define the internal thermal convection coefficients. The flow in the ducts is supposed fully developed. Different geometries are used by the manufacturer of the bipolar. The geometries in the main and secondary cooling ducts are circular and rectangular for the ducts in the cell. In the two first configurations, the Colburn correlation [8] is used. It is expressed thanks to Eq. (6) where the flow is turbulent:

$$Nu = 0.023\, Re^{0.8}\, Pr^{1/3} \tag{6}$$

where the Reynolds number is defined as

$$Re = \frac{u_m x}{\nu} \tag{7}$$

and the Prandtl number expressed as:

$$Pr = \frac{\nu}{a} \tag{8}$$

Pr is calculated at the arithmetic average temperature of water between the inlet and the outlet of the cooling system. The ducts in channels 1–3 are rectangular. Mass flow is considered as laminar flow (small value of Re). In that case, correlation (9)

Table 2
Thermal conductivities of the materials of the cell

Bipolar plates (carbon), λ_c (W m^{-1} K^{-1})	20
Diffusion layer, λ_{diff} (W m^{-1} K^{-1})	0.1
Membrane, λ_{mem} (W m^{-1} K^{-1})	0.6

permitting to determine the Nusselt number issued from Shah and London [9] is used:

$$Nu = 7.541(1 - 2.610\zeta + 4.970\zeta^2 - 5.119\zeta^3 + 2.702\zeta^4 - 0.548\zeta^5) \quad (9)$$

with a shape coefficient ζ of 0.7 defined as the ratio of the length of the cell along the axes O, x and O, y (Fig. 2).

Nusselt numbers permit to calculate the heat transfer coefficients by free convection on the external surface of the cell. Nu depending on the surface temperatures, an iterative method has then been used in configurations 2 and 3. At each step, it has been calculated with the new value of the temperature issued from the precedent step of the computation. The convergence is accepted for a 0.1% variation of temperature. Then, for $4.2 \times 10^6 < Ra < 7.6 \times 10^6$ [10], Nu is given by Eq. (10) for the horizontal surface at the top of the cell:

$$Nu = 0.27 Ra^{1/4} \quad (10)$$

with

$$Ra = Gr\, Pr = \frac{g\beta|T_p - T_\infty|x^3}{a\nu}. \quad (11)$$

T_p is the wall temperature and T_∞ is the temperature of the external surrounding:

β is defined as:

$$\beta = \frac{2}{T_p + T_\infty} \quad (12)$$

For the horizontal surface at the bottom of the cell, the Nusselt number is also given by Eq. (13) [11]:

$$Nu = 0.54 Ra^{1/4}. \quad (13)$$

For vertical surfaces, the corresponding Nusselt number is given by (14), considering a laminar flow [12]:

$$Nu = 0.59 Ra^{1/4}. \quad (14)$$

The coefficient of heat transfer by convection permitting to estimate the conductances is obtained from Eq. (15):

$$h = \frac{Nu\, x}{\lambda_{fl}} \quad (15)$$

with x the characteristic length of the considered surface.

6. Results

Solved equations are given thanks to expression (2). Expressions of Eqs. (2a)–(2c) are obtained with precedent dimensionless numbers.

Three loaded experimental tests (0.3, 0.4 and 0.5 A cm^{-2}) are presented with their corresponding modeling for the output temperature regulated at 50 °C. Other experimental phases with no load are realized for 40, 50 and 60 °C as output water temperatures. The reason of the constant temperature of the water for the tests with load is to particularize the internal power sources of the cell as function of the load. Indeed, it is fundamental for understanding the electrical, chemical and thermal behaviors of the cell with the load to freeze all the other parameters and especially the high influence of the water temperature. At the opposite, with no load, the modification of the water temperature considered as the functioning temperature of the cell permits to define the unknown internal thermophysical parameters as the thermal conductivities or the thermal contact resistances necessary for the modeling. For these six modeling, we describe the external temperatures so that the 3D internal and external heat fluxes. Two PEMFC of 3 and 20 cells with respective power of 150 and 500 W are studied. Fig. 4 gives the results of measured and computed temperatures of tests without load for different input temperatures of the water. Curve in configuration 1 gives the measured temperatures obtained thanks to the infrared camera on the isothermal surfaces of the stack (3 cells) with temperatures of the cooling water given at 40, 50 and 60 °C. Two other curves give the computed temperatures for respectively configurations 2 and 3.

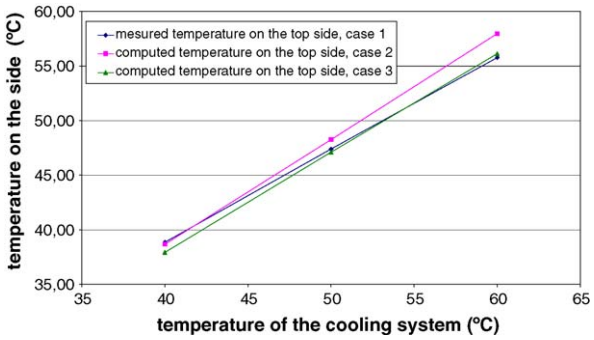

Fig. 4. Temperatures as functions of water temperature. Top surface, without load, 3 cells.

The three profiles are rectilinear. Differences of measured and computed temperatures on the top surface of the stack do not exceed 2.5 °C for the temperature of the water at 50 °C.

Fig. 5 gives the same computed and measured temperatures with loads at 0.3, 0.4 and 0.5 A cm^{-2}. The differences between the measured and the computed values are then smaller and do not exceed 1.5 °C. Nu obtained from Eq. (13) are 28.

Fig. 6 gives the same results as Fig. 5 for the 20 cells stack. Differences of the measured and the computed values are similar as for the 3 cells stack (about 1.3 °C for a temperature of the water of 50 °C. The temperature at the top surface decreases as

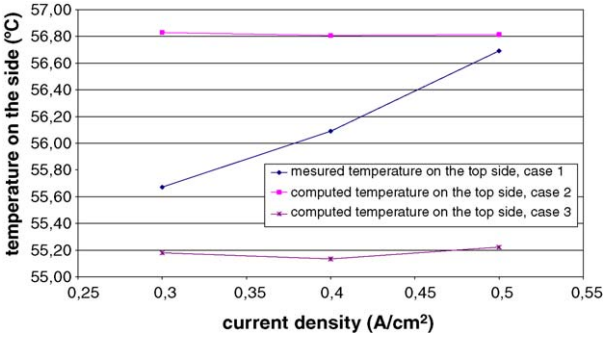

Fig. 5. Temperature on the top side, with load, 3 cells.

Table 3
Characteristics of the flow in the main duct

	40 °C	50 °C	60 °C
Without load			
3 cells			
ΔT (°C)	1	0.6	0.9
Flow rate (l min^{-1})	1.06	1.09	0.91
	0.3 A cm^{-2}	0.4 A cm^{-2}	0.5 A cm^{-2}
With load (T = 50 °C)			
3 cells			
ΔT (°C)	0.2	−0.3	−0.6
Flow rate (l min^{-1})	1.02	1.00	1.08
20 cells			
ΔT (°C)	0.9	−0.1	−1.3
Flow rate (l min^{-1})	2.41	2.47	2.45

the current density increases. Indeed, the operating temperature is controlled with the output temperature of the cooling system. The heat released by the electrochemical reaction increases with the current density. The input temperature of the cooling system decreases as considering constant the output temperature. As the current density increases, the electrochemical reaction produces more heat. Temperatures of the stack tend to become higher as the temperature of the feeding system. This effect is more important for the 20 cells stack where the heat released by the electrochemical reaction is more important than for the 3 cells stack.

Finally, after having integrated modeled thermal fluxes of the cell on the entire PEMFC, the balance of power of the considered cell is done. To reach that result, it is necessary first of all to estimate experimentally the heat fluxes transferred through the water duct. The heat fluxes transferred to the other fluids are considered as negligible. Indeed, the experimental values obtained at the higher load at 50 °C are respectively 0.7 and 1.8 W for one cell (case of the 3 cells stack) for the hydrogen and the air ducts. The sum of these ones does not exceed 7% of the heat power transferred with all the fluids. Table 3 gives the experimental results with ΔT as the difference of the input and output temperatures of water.

Table 4 is the power balance according to the first law of thermodynamic for the three configurations. The positive algebraic values are relative to gaining of power in comparison to the negative values for power losses by the stack. Table 5 gives the different computed leak conductances to balance the thermal power sources in the stacks for the three configurations.

Table 4
Energy balance of the stack

Load (T = 50 °C)	0.3 A cm^{-2}	0.4 A cm^{-2}	0.5 A cm^{-2}
3 cells			
Chemical (W)	112.96	150.50	187.82
Electrical (W)	−60.23	−72.89	−85.74
Thermal (W)	−52.73	−77.61	−102.08
20 cells			
Chemical (W)	749.35	998.64	1253.47
Electrical (W)	−401.80	−514.24	−640.85
Thermal (W)	−347.54	−484.40	−612.62

Table 6 gives the same computed parameter for the two stacks with load, the stack is regulated at 50 °C.

It can be seen in Table 6 that the leak conductance becomes smaller as the current density increases. The relative part of heat transfer extracted from the stack by the cooling system increases. The input temperature of the cooling system increases as the current density is smaller, being also more efficient. The leak conductances for the configuration 3 are then smaller compared to the other configurations. The taking into account of the boundary conditions defined in configuration 3 between two adjoining cells, creates a heat flux on the axes O, z which reduces the part of the heat lost with the other kinds of heat transfer.

Fig. 7 quantifies the heat fluxes of one computed cell from the cathode bipolar plate to the anode bipolar plate of the next (fictive) cell. These thermal fluxes are expressed as functions of the current densities produced by the cell.

The two curves are relative to the two stacks. Configurations 1 and 2 are finally similar considering that they do not allow heat losses by conduction in direction O, z (homogeneous Neumann conditions and cyclical conditions). For that reason,

Table 5
Leak conductances, without load, 3 cells

	40 °C	50 °C	60 °C
Configuration 1 (W K^{-1})	2.18	0.86	0.71
Configuration 2 (W K^{-1})	2.19	0.87	0.73
Configuration 3 (W K^{-1})	1.75	0.44	0.31

Table 6
Leak conductances, with load, 3 and 20 cells

	0.3 A cm^{-2}	0.4 A cm^{-2}	0.5 A cm^{-2}
3 cells			
Configuration 1 (W K^{-1})	0.88	0.80	0.78
Configuration 2 (W K^{-1})	0.89	0.80	0.78
Configuration 3 (W K^{-1})	0.44	0.35	0.32
20 cells			
Configuration 1(W K^{-1})	7.09	6.79	5.95
Configuration 2 (W K^{-1})	7.09	6.79	5.95
Configuration 3 (W K^{-1})	7.02	6.72	5.88

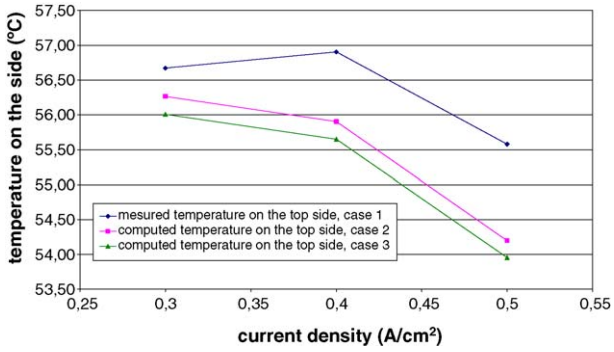

Fig. 6. Temperature on the top side, loaded tests, 20 cells.

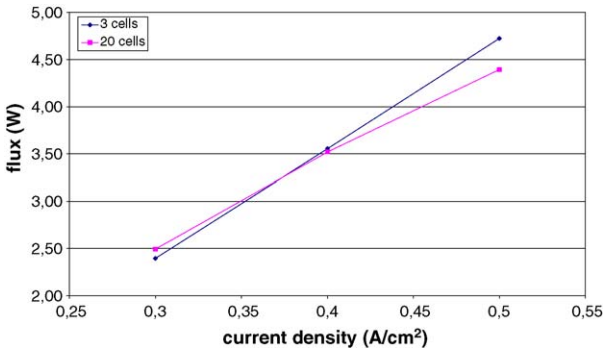

Fig. 7. Heat flux from the cathode bipolar plate to the anode bipolar plate, in configurations 1 and 2.

configuration 3 is the more realistic case, but it is very difficult to quantify with a very good accuracy.

Figs. 8 and 9 show respectively the heat transfer in the direction O, z for one computed cell for both stacks. The heat fluxes are lost for the system and dispelled to the external medium. They are expressed as a function of the current densities (configuration 3). The difference of the influence of the cooling fluid can be seen on both figures through the values of the flux. It is shown in that way the high influence of the cooling system for the stack of 20 cells (as shown in following Table 8). Thermal conductances between the stack and the external medium are defined as a function of the number of cells for each stack. Consequently, the axial heat flux is higher for the 3 cells stack than for the 20 cells stack.

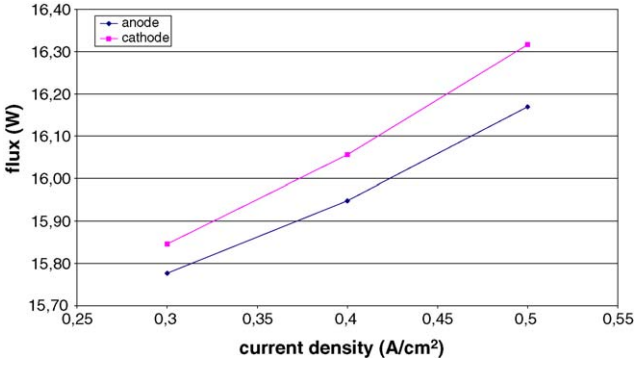

Fig. 8. Heat flux to external medium in "z" axis, case 3, with load, 3 cells.

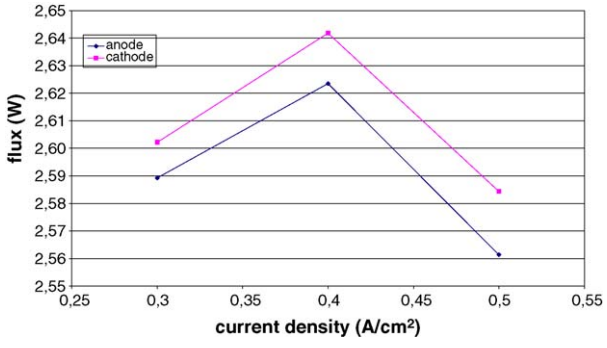

Fig. 9. Heat flux to external medium in "z" axis, configuration 3, with load, 20 cells.

Table 7
Heat energy extracted by the cooling system

	0.3 A cm^{-2}	0.4 A cm^{-2}	0.5 A cm^{-2}
3 cells (%)	22.2	−24.6	−43.4
20 cells (%)	42.8	−2.7	−35.4

Table 8
Heat energy extracted by the cooling system

	0.3 A cm^{-2}	0.4 A cm^{-2}	0.5 A cm^{-2}
3 cells			
Configuration 1	−86.3	−88.7	−88.6
Configuration 2	−88.9	−90.1	−89.5
Configuration 3	85.7	29.7	2.5
20 cells			
Configuration 1	−88.6	−90.2	−90.2
Configuration 2	−90.4	−91.6	−90.9
Configuration 3	−62.3	−71.2	−75.2

Tables 7 and 8 compare and quantify the relative influence of the cooling system at different current densities for one cell and all the cells of the two stacks. As shown in Table 7, both stacks are not able to reach the operating temperature at 0.3 A cm^{-2}. The "cooling" system is then a heater system. Table 8 describes the dissipation way of the heat. Configurations 1 and 2 in both stacks are similar.

When heat cannot be dispelled in the axial axis O, z because the modeling does not take into account this possibility (configurations 1 and 2), the cooling channels are the main processes to extract the heat. Heat transfers by conduction along axes O, x and O, y are not very important, particularly for the configuration 2 with the computed wall temperatures. The configuration 3 takes into account the heat flux on axis O, z. For the 3 cells stack, the cooling channels are in fact some heaters for all values of the current density. It is not realistic. For the 20 cells stack, even in the configuration 3, the heat flux is mainly removed by the cooling channels. The thermal conductance in O, z axis is not a linear function of the number of cells and the effective thermal conductance is smaller than the physical thermal conductance computed from the different components of one cell.

In both Tables 7 and 8, the positive values correspond to contribution of power and negative values to the heat losses when considering the stack as a thermodynamical system.

7. Discussion

Heat transfers in the stack change with the operating conditions. When the stack operates without load (3 cells stack), the feeding system is used to reach the operating temperature. For a water output temperature regulated at 40 °C, the heat flux between two cells is negligible. Indeed, the difference of temperatures between the wall and the external air is about 15 °C. The different cells also operate under adiabatic conditions (configuration 2). As the temperature of the water increases the heat fluxes in the axis O, z follow the same evolution. The stack operates also according to the third configuration. For a current density of 0.3 A cm^{-2}, the heat quantity created by the

electrochemical reaction stays insufficient to maintain constant the operating temperature. The heat power released by the electrochemical reaction is also extracted by conduction. The feed system then behaves as a heater system. The boundary conditions of the cells stay near to those modeled in configuration 3. With load, the heat released by the electrochemical reaction increases with the current density. For a current density of $0.4\,A\,cm^{-2}$ the feed system extracts the heat generation for the three cells stack whereas the equilibrium of fluxes is quite reached for the twenty cells stack (Table 7). As the current density goes up, it can be seen a difference of temperatures of the system between the configurations 3 and 2. It means that the system moves to an adiabatic mode. For the 20 cells stack, it can be observed a small difference between configurations 2 and 3. Indeed, the thermal conductivity is supposed inversely proportional to the number of the cells. It is estimated to about $0.02\,W\,m^{-1}\,K^{-1}$ for the 20 cells stack whereas it was about $0.15\,W\,m^{-1}\,K^{-1}$ for the 3 cells stack. Nevertheless, the wall temperatures computed are lower than the measured temperatures. The internal heat fluxes distributions are different between the two stacks because of the important differences of the geometries at the origin of different internal thermo physical parameters (convective coefficients so that equivalent thermal conductivities).

8. Conclusion

To realize the thermal modeling of a PEMFC, it is necessary to predict internal temperatures reached for different functioning configurations. Finally, the global efficiency of the cell with its feed system can be estimated. To validate the model developed for one cell (instead of 3 or 20), it has been necessary to obtain the convergence of computed and simulated temperatures at the output of the cooling water. The approach is particularly complicated in reason of the relative absence of experimental measurements on the stack. The validation of the modeling tool is realized for different input temperatures of water (without load) and with different loads ranging from 0.3 to $0.5\,A\,cm^{-2}$. The output temperature of the cooling channel is regulated and also considered as constant at 50 °C. The validated tool has also permit to estimate the internal and external ways of heat transfer. Studies of one cell and for the entire stack (3 and 20 cells) and their integration in a global thermal behavior model will then permit to estimate the final efficiency of the stack with the feed system. Next step, according to the important losses and non utilized external heat fluxes, will consist in the development of the utilization of this power on the test bench to optimize the efficiency of the stack with its feed system. For this it is necessary to modelize more than one cell in order to take into account the influence of the neighboring cells to consider the heat flux distribution.

References

[1] T.V. Nguyen, R.E. White, A water and heat management model for proton-exchange-membrane fuel cells, J. Electrochem. Soc. 140 (8) (1993) 2178–2186.
[2] J.S. Yi, T.V. Nguyen, An along the channel model for proton exchange membrane fuel cells, J. Electrochem. Soc. 145 (4) (1998) 1149–1159.
[3] W.M. Yan, F. Chen, H.Y. Wu, C.Y. Soong, H.S. Chu, Analysis of thermal and water management with temperature-dependent diffusion effects in membrane of proton exchange membrane fuel cells, J. Power Sources 129 (2004) 127–137.
[4] H. Ju, H. Meng, C.Y. Wang, A single-phase, non-isothermal model for PEM fuel cells, Int. J. Heat Mass Transfer 48 (2005) 1303–1315.
[5] J.B. Saulnier, La modélisation thermique et ses applications aux transferts couplés et au contrôle actif, Thèse de Doctorat ès Sciences Physiques de l'Université de Poitier, 1980.
[6] L. Dumercy, R. Glises, H. Laouhlia Gualous, J.M. Kauffmann, Transient Thermal Computation of a PEM Fuel Cell by a Nodes Modeling, IEEE, VTC Fall, Orlando, USA, 2003.
[7] M. Necati Ozisik, Heat Transfer — A Basic Approach, McGraw-Hill International Editions, 1985.
[8] A.P. Colburn, A method of correlating forced convection heat transfer data and comparison with fluid friction, Trans. Am. Inst. Chem. Eng. 29 (1933) 174–210.
[9] R.K. Shah, A.L. London, Laminar flow forced convection in ducts, in: Advanced in Heat Transfert, Supplement 1, Academic Press, 1978.
[10] T. Fudjii, H. Imura, Natural convection heat transfer from plate with arbitrary inclination, Int. J. Heat Mass Transfer. 15 (1972) 755–767.
[11] M. Fishenden, O.A. Saunders, An Introduction to Heat Transfer, Oxford University Press, Oxford, 1950.
[12] W.H. Mc Adams, Transmission de la chaleur, Dunod, 1961.